Acta Pharmaceutica Sinica B 2022;12(9):3694–3709

Chinese Pharmaceutical Association
Institute of Materia Medica, Chinese Academy of Medical Sciences

Acta Pharmaceutica Sinica B

www.elsevier.com/locate/apsb
www.sciencedirect.com

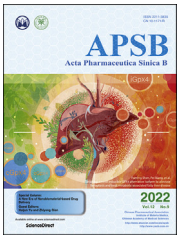

ORIGINAL ARTICLE

Combining immune checkpoint blockade with ATP-based immunogenic cell death amplifier for cancer chemo-immunotherapy

Jiulong Zhang[a], Xiaoyan Sun[a], Xiufeng Zhao[b], Chunrong Yang[c], Menghao Shi[a], Benzhuo Zhang[d], Haiyang Hu[a], Mingxi Qiao[a], Dawei Chen[a], Xiuli Zhao[a,*]

[a]*School of Pharmacy, Shenyang Pharmaceutical University, Shenyang 110016, China*
[b]*Department of Oncology, Affiliated Hongqi Hospital of Mudanjiang Medical College, Mudanjiang 157011, China*
[c]*Department of Pharmacy, Shantou University Medical College, Shantou 515041, China*
[d]*Department of Neurology, The Second Affiliated Hospital of Mudanjiang Medical College, Mudanjiang 157009, China*

Received 4 January 2022; received in revised form 21 February 2022; accepted 6 April 2022

KEY WORDS

Immunogenic cell death amplifier;
ATP;
Fenton reaction;
Immune checkpoint blockade;
Coordination polymer nanoparticles;
pH/ROS sensitive;
Phenylboric acid

Abstract Amplifying "eat me signal" during tumor immunogenic cell death (ICD) cascade is crucial for tumor immunotherapy. Inspired by the indispensable role of adenosine triphosphate (ATP, a necessary "eat me signal" for ICD), a versatile ICD amplifier was developed for chemotherapy-sensitized immunotherapy. Doxorubicin (DOX), ATP and ferrous ions (Fe^{2+}) were co-assembled into nanosized amplifier (ADO-Fe) through $\pi-\pi$ stacking and coordination effect. Meanwhile, phenylboric acid-polyethylene glycol-phenylboric acid (PBA-PEG-PBA) was modified on the surface of ADO-Fe (denoted as PADO-Fe) by the virtue of D-ribose unit of ATP. PADO-Fe could display active targetability against tumor cells *via* sialic acid/PBA interaction. In acidic microenvironment, PBA-PEG-PBA would dissociate from amplifier. Moreover, high H_2O_2 concentration would induce hydroxyl radical ($\cdot OH$) and oxygen (O_2) generation through Fenton reaction by Fe^{2+}. DOX and ATP would be released from the amplifier, which could induce ICD effect and "ICD adjuvant" to amplify this process. Together with programmed death ligands 1 (PD-L1) checkpoint blockade immunotherapy, PADO-Fe could not only activate immune response against primary tumor, but also strong abscopal effect against distant tumor. Our simple and multifunctional ICD amplifier opens a new window for enhancing ICD effect and immune checkpoint blockade therapy.

*Corresponding author. Tel.: +86 24 23986306.
E-mail address: raura3687yd@163.com (Xiuli Zhao).

Peer review under responsibility of Chinese Pharmaceutical Association and Institute of Materia Medica, Chinese Academy of Medical Sciences

https://doi.org/10.1016/j.apsb.2022.05.008

1. Introduction

In developing and developed countries, cancer is a main cause of death for human beings[1−3]. Compared with traditional chemotherapy, immunotherapy has emerged as a hot spot in current field[4−7]. Immune checkpoint blockade therapy (programmed death 1 or programmed death ligand 1, abbreviated as PD-1 and PD-L1) received increasing concern for its capability of T cell regulation to activate antitumor immune response[8−10]. It has been demonstrated that such approach could sufficiently inhibit tumor growth against high tumor-specific T cells infiltration tumor (named as hot tumor)[11,12]. However, its clinical outcomes are insufficient for repressed T cells infiltration tumor (named as cold tumor) due to its tumor immunosuppressive microenvironment (TIM) together with low immunogenicity[13,14]. Therefore, increasing tumor immunogenicity together with reversing TIM is considered as a promising approach for tumor immunotherapy.

Recent reports prove that some anthracyclines molecules such as doxorubicin (DOX) serve not only as chemodrug for directly inducing DNA damage, but also a potential immunogenic cell death (ICD) inducer[15,16]. Dying tumor cells with DOX administration can induce endoplasmic reticulum (ER) stress response and autography. ER stress can induce calreticulin protein (CRT) translocation on cell surface and thereby generating "eat me signal" for dendritic cells (DCs) recognition[17−19]. Autography can increase adenosine triphosphate (ATP) release from dying cells, which serves as 'find me signal' for DCs recruitment. Moreover, high mobility group box 1 (HMGB1) can also be released into extracellular space to bind Toll-like receptor 4 (TLR4) on DCs and amplify its antigen presenting capability[20,21]. Above three steps are indispensable for ICD, which subsequently increase DCs maturation and T cells infiltration. ATP, serves as 'find me signal' for DCs recruitment, is the initial process for DCs activation and its concentration correlates positively to DCs recruitment efficacy. We hypothesized that increasing ATP accumulation in tumor regions would facilitate ICD efficacy. However, ATP, act as a source of energy, is ubiquitous. How to target delivery of ATP to tumor region is challenging.

Despite promising DOX-based ICD strategy, which could efficiently modulate tumor innate immunity for PD-1/PD-L1 therapy, T cell infiltration is severely restricted by TIM as tumor has many immune escape mechanisms[22−26]. Therefore, remodeling TIM can further activate antitumor immune response. Tumor-associated macrophage (TAM), as one of the most important cell subpopulations in solid tumor, plays a crucial role in TIM, which is also positively correlated to tumor metastasis and invasion[27,28]. TAM is divided into two phenotypes, anti-tumor M1-TAM and pro-tumor M2-TAM. Furthermore, most TAM in solid tumor is M2 phenotype, leading to tumor proliferation[29,30]. Meanwhile, hypoxia tumor microenvironment also facilitate M2 phenotype polarization of TAM[31]. Therefore, an ideal strategy for cancer immunotherapy should not only induce tumor ICD effect, but also polarize TAM from M2 to M1 and relieve hypoxia microenvironment to reverse TIM.

Despite many clinical outcomes for DOX with antitumor immune response activation, highly effective administration of DOX is restricted by its poor tumor biodistribution and severe cardiac toxicity. Many DOX-based drug delivery systems are reported to have more advantages such as biocompatibility, tumor targetability and stimuli-responsive drug release capability[32]. Nevertheless, they were always confronted with some difficult problems such as complex design, low drug-loading efficacy as well as high cost. Therefore, it is urgent to discover novel drug delivery system with facile synthesis procedure, high loading capability and multi-physiological functions. To the best of our knowledge, multi-functional drug delivery system, which could induce ICD cascade, polarize M1 TAM and relieve hypoxia tumor microenvironment, is urgently needed but rarely reported.

To solve the aforementioned problems, a "multi-in-one" ICD amplifier (named as PADO-Fe) was prepared for cancer chemotherapy-sensitized immunotherapy. As illustrated in Scheme 1A, this ICD amplifier was constructed by self-assembly of DOX, ATP and ferrous ions (Fe^{2+}) through $\pi-\pi$ stacking and coordination effect. Owing to 'find me signal' of ATP during ICD cascade, we hypothesized that intertumoral delivery of ATP could amplify ICD process through increasing ATP release from dying tumor cells, which could elevate DCs recruitment and maturation. Fe^{2+}, served as an essential trace metal element, is relatively safe for intravenous administration. Fe^{2+} could coordinate with carbonyl/amine or phosphate groups of DOX and ATP to form metal−organic complex (MOC). Furthermore, Fe^{2+} could also catalyze H_2O_2 to highly toxic ·OH and oxygen, known as Fenton reaction[33], which would both relieve tumor hypoxia and possess tumor chemodynamic therapy (CDT)[34]. Moreover, Fe^{2+} could reverse TAM phenotype from M2 to M1 to reverse TIM and activate antitumor immune response[35,36]. In order to enhance *in vivo* circulation time and tumor targetability, PBA-PEG-PBA was modified on the surface of ADO-Fe through simple mixing process, which could interact with ADO-Fe through vicinal diols structure of versatile ATP molecule. After i. v. injection of PADO-Fe, this amplifier was accumulated into tumor sites *via* EPR effect. Subsequently, PADO-Fe could be internalized into tumor cells through sialic acid residues-mediated endocytosis and response to intracellular pH/H_2O_2 microenvironment. PBA-PEG-PBA would dissociate from PADO-Fe due to reversible binding of PBA and vicinal diols structure from ATP. Meanwhile, Fe^{2+} would catalyze H_2O_2 to toxic ·OH and O_2 *via* Fenton reaction. Of special note, endogenous O_2 microbubbles would facilitate dissociation of nanoparticle, thereby reach stimuli-responsive DOX/ATP release. Not only free DOX in cytoplasm could directly kill tumor cells, dying cells could also release damage-associated molecular patterns (DAMPs) to induce ICD cascade. Furthermore, intracellular high concentration ATP from PADO-Fe would also amplify this process. ATP secretion, CRT expression and HMGB1 release would recruit immature DCs to mature DCs for antigen presenting. PD-L1 antibody-mediated immune checkpoint blockade and Fe^{2+}-mediated TAM phenotype transition (M2 to M1) would both reverse TIM, contributing to activating effector T cells proliferation and infiltration for immunotherapy against primary and

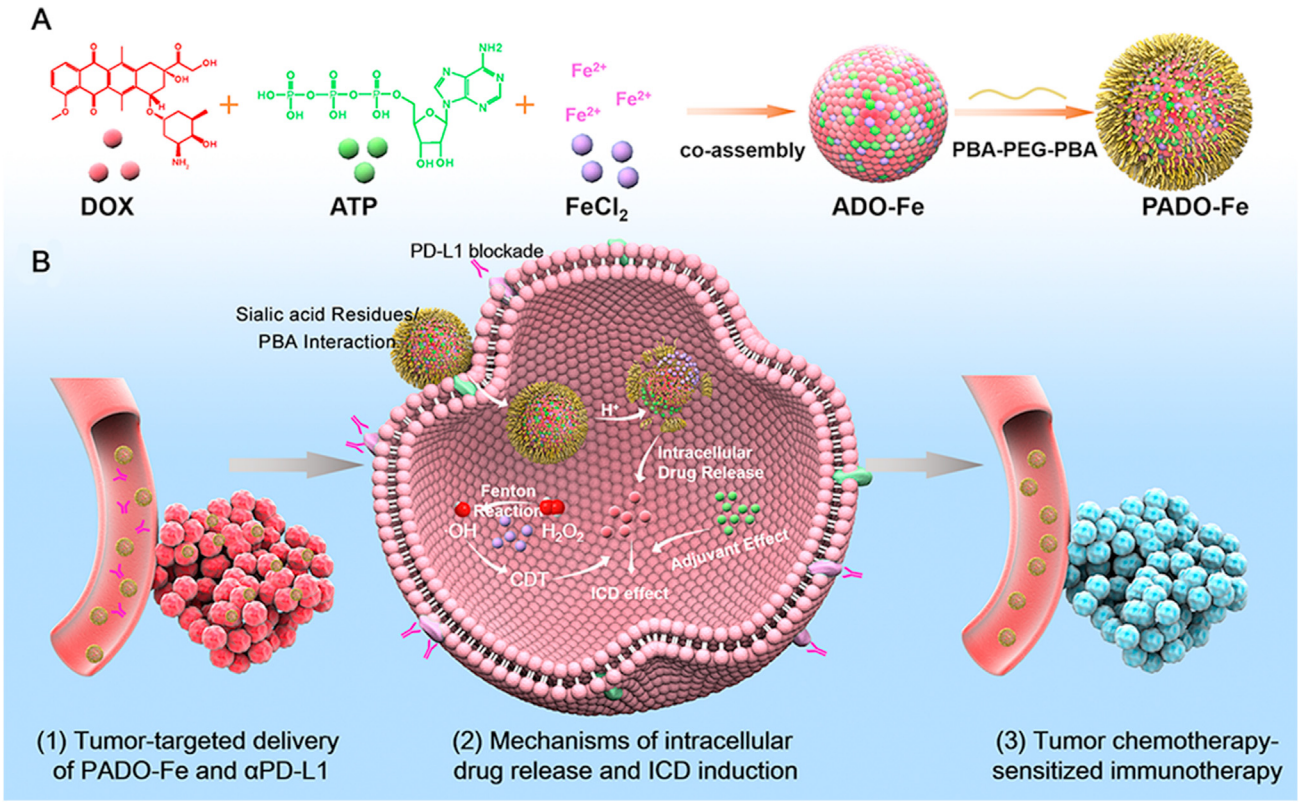

Scheme 1 Schematic illustration of immunogenic cell death amplifier for sensitizing PD-L1 checkpoint blockade immunotherapy and its potential mechanism. (A) Co-assembly process of PADO-Fe was presented through $\pi-\pi$ stacking and coordination effect; (B) the potential mechanism of PADO-Fe for tumor-targeted delivery, intracellular drug release and ICD induction in combination with immune checkpoint blockade for tumor chemotherapy-sensitized immunotherapy.

distant tumors. Overall, this ICD amplifier proposes a unique platform for combination immune checkpoint blockade therapy and a new insight for ATP as an 'ICD adjuvant' in cancer chemotherapy-sensitized immunotherapy.

2. Materials and methods

2.1. Reagents

PBA-PEG-PBA was synthesized by our lab. Doxorubicin hydrochloride (DOX·HCl), ferrous chloride tetrahydrate ($FeCl_2 \cdot 4H_2O$), adenosine triphosphate disodium (ATP) and benzoic acid (BA) were purchased from Aladdin (Shanghai, China). 2,7-dichlorodihydrofluorescein diacetate (DCFH-DA) was supplied from Sigma−Aldrich (USA). CD3-PerCP Cy5.5 (clone: 145-2C11), CD4-FITC (clone: GK1.5), CD8-PE (clone: 53−6.7), CD11c-FITC (clone: N418), CD80-PE (clone: 16-10A1), CD86-APC (clone: GL-1), CD11b-FITC (clone M1/70), CD206-PE (clone C068C2), F4/80-APC (clone BM8.1) were all purchased from Biolegend (USA). CRT primary antibody (ab92516), HMGB1 primary antibody (ab18256), HIF-1α primary antibody (ab279654) and ki-67 primary antibody (ab15580) were all purchased from Abcam (USA). IL-6, TNF-α, IFN-γ ELISA kit were purchased from Abcam (USA).

2.2. Studies in cells and animals

4T1 murine breast cancer cell line was cultured in RPMI-1640 medium supplemented with 10% FBS at 37 °C in 5% CO_2 atmosphere. Bone marrow of BALB/c mice was used to obtain immature DCs according to the literature[37]. Briefly, bone marrow of femurs and tibias was collected and washed, followed by GM-CSF stimulation and IL-4 polarization.

BALB/c mice (female, 16−18 g) were purchased from Huafukang Biotechnology Co., Ltd. (Beijing, China) For the construction of 4T1 tumor-bearing mice, 4T1 tumor cells (10^6 4T1 cells in 0.2 mL of PBS) were subcutaneously injected in the leg regions. When the tumor volume reached approximately 100 mm^3, they were randomly divided into several groups for further study. All animal work was approved by Institution Animal Care and Use Committee of Shenyang Pharmaceutical University.

2.3. Preparation and characterization of different nanoparticles

To prepare PADO-Fe, ADO-Fe core was first constructed. Briefly, 10.8 mg of DOX and 5.1 mg of ATP were dispersed in 2 mL of pure water, then a gradient concentration of $FeCl_2$ solution (dissolved in pure water) was added droplet into the system with constant stirring for 2 h. Thereafter, the mixture was centrifuged at 10,000 rpm (Beckman Coulter, Allegra X-30, Kraemer Boulevard Brea, CA, USA) for 30 min to collect nanoparticles. Precipitation was washed with pure water to obtain ADO-Fe. To prepare PADO-Fe, ADO-Fe was suspended in pure water and 2% (*w*/*w*) PBA-PEG-PBA was added into the system and stirred for 1 h. The mixture was centrifuged to collect nanoparticles and unreacted PBA-PEG-PBA was removed. Cy3-labeled nanoparticles were prepared using the same way except 1% DOX was replaced by Cy3-diNHS ester. The content of DOX and ATP was measured by

high performance liquid chromatography (HPLC) and Fe^{2+} was measured using inductively coupled plasma mass spectrometry (ICP-MS).

2.4. Drug release

To investigate drug release behavior of different nanoparticles, 1 mL of different samples were placed into a dialysis bag (MWCO 1.0 kDa). The bags were placed into 100 mL of different release medium (PBS pH 7.4, PBS pH 6.8 and PBS pH 6.8 + 1% H_2O_2) with constant stirring at 37 °C. At interval time, 1 mL of release medium was taken for content analysis and equal volume of fresh medium was added. The accumulative drug release profile was calculated according to the equation as references reported[38].

2.5. Detection of O_2 generation

Dissolved oxygen meter was used to detect oxygen generation of different nanoparticles. Briefly, 5 mL of different samples were prepared and H_2O_2 (1%) was added into each sample. Subsequently, samples were placed in a water bath at 37 °C. At interval time pint, oxygen concentration was measured.

Meanwhile, $[Ru(dpp)_3]Cl_2$ was used for observing oxygen generation in cellular level. Briefly, 4T1 cells were seeded into 6-well plate for 12 h to allow attachment. Subsequently, the cells were cultured in hypoxia condition and different nanoparticles were added into each well for 6 h. $[Ru(dpp)_3]Cl_2$ (10 μg/mL) was added into the medium and cultured for another 12 h. The cells were washed with PBS and finally observed using confocal laser scanning microscopy (CLSM).

2.6. Detection of ·OH generation

BA, which could react with ·OH to form highly fluorescent product, was used to measure the generation of ·OH[39]. Briefly, H_2O_2 (1%) was added into different samples and incubated at 37 °C. At interval time point, samples were collected, and BA solution (0.5 mmol/L) was added into the samples. Finally, the samples were centrifuged at 10,000 rpm (Beckman Coulter, Allegra X-30, Kraemer Boulevard Brea, CA, USA) for 30 min and the absorbance of supernatant was measured at 435 nm.

2.7. Cellular uptake assay

Flow cytometry and confocal laser scanning microscopy (CLSM) were both used for investing cellular uptake capability of different formulations. In a typical procedure, for flow cytometry assay, 4T1 cells were seeded into 6-well plate for 12 h to allow attachment. Different nanoparticles (DOX: 10 μg/mL) were added into each well and incubated for 4 h. Thereafter, cells were collected using trypsin, washed with cold PBS for 3 times and finally measured using flow cytometry. For CLSM assay, cells were seeded into glass-covered 6-well plate to allow attachment. Different nanoparticles were added into each well and incubated for 4 h. Subsequently, cells were washed with PBS, fixed with 4% paraformaldehyde and stained with Hoechst 33258. Cellular fluorescence of different samples was observed by CLSM.

2.8. Cell cytotoxicity assay

MTT assay was used to evaluate cell cytotoxicity of different nanoparticles in the absence/presence of H_2O_2. 4T1 cells were seeded into 96-well plate overnight. Then the medium was removed, and gradient concentration nanoparticle-dispersed culture medium was added into each well and allowed to incubate for 24 h. Thereafter, 20 μL of MTT solution (5 mg/mL) was added into each well and incubated for another 4 h. Finally, all medium was removed and 100 μL of DMSO was added for measuring the optical density (OD) at 580 nm. Cell viability was calculated according to Eq. (1):

$$\text{Cell viability } (\%) = (OD_{sample} - OD_{blank}) \times 100 / (OD_{control} - OD_{blank}) \quad (1)$$

Annexin V-FITC/PI apoptosis kit was applied to measure apoptosis-inducing capability of different nanoparticles in both physiological and H_2O_2 environment. Briefly, 4T1 cells were seeded into 6-well plate and incubated overnight. Different nanoparticles (10 μg/mL of DOX) were added into each well and incubated for 24 h. Subsequently, cells were collected, washed with PBS, stained with annexin V-FITC/PI and finally measured by flow cytometry.

2.9. In vitro ICD induction assay

2.9.1. DCs maturation assay

Conventional Transwell model was established to investigate DCs maturation. Briefly, 4T1 tumor cells were seeded into 6-well plate and incubated with different nanoparticles for 4 h. Thereafter, the cells were washed with PBS three times and collected. Meanwhile, immature DCs were cultured in the lower chamber while drug-treated 4T1 tumor cells were seeded in upper chamber. The cells were co-cultured for 12 h and cells of lower chamber were collected and washed with PBS three times. The cells were re-suspended in flow cytometry staining buffer (FCSB) and cocktail antibodies were added into each sample. The samples were measured using flow cytometry and matured DCs were gated as $CD11c^+CD80^+CD86^+$.

2.9.2. ATP content assay

ATP content was measured using commercially available ATP-measuring kit. Briefly, 4T1 cells were seeded into 12-well plate. Different nanoparticles were added into each well and incubated for 12 h (10 μg/mL of DOX). Subsequently, the medium was removed, and the cells were collected and washed. The following operations were according to the manufacturer of the kit.

2.9.3. HMGB1 and CRT expression

HMGB1 and CRT immunofluorescence was investigated to observe their biodistribution level. In a typical procedure, 4T1 cells were seeded into glass-covered 6-well plate to allow attachment. Different nanoparticles were added into each well and incubated for 12 h. Subsequently, cells were washed with PBS, fixed with 4% PFA and visualized nuclei with Hoechst 33258. For HMGB1 and CRT immunofluorescence, cells were permeabilized with 0.1% Triton X-100, washed with PBS and blocked with goat serum. Then anti-CRT and anti-HMGB1 primary antibodies were separately incubated with cells overnight at 4 °C. Cells were finally stained with goat anti-rabbit IgG H&L (Alexa Fluor® 488, ab150077) for another 1 h and observed by CLSM.

2.10. In vitro detection of ROS generation

DCFH-DA was used as a fluorescence probe to detect intracellular ROS generation when the cells were treated with different nanoparticles. Briefly, cells were seeded in 6-well plate overnight and treated with different nanoparticles (10 μg/mL DOX) for 12 h. After washing with PBS, DCFH-DA (10 μmol/L) was added and incubated for another 1 h. Cells were washed with PBS, fixed with 4% PFA, stained with Hoechst 33258 and finally visualized by CLSM.

2.11. In vivo biodistribution assay

IVIS system was used to observe the biodistribution behavior of different nanoparticles and Cy3 DiNHS ester was used as fluorescence probe. Tumor-bearing mice were intravenously administrated with different Cy3-labeled nanoparticles and at interval time point, biodistribution behavior of nanoparticles was visualized through IVIS system.

2.12. In vivo antitumor activity

4T1 tumor-bearing mice were randomly divided into several groups including control, free DOX, DO-Fe, ADO-Fe, PADO-Fe and PADO-Fe plus aPD-L1, and the concentrations of DOX and aPD-L1 were 2 and 1 mg/kg, respectively. Different nanoparticles/aPD-L1 were intravenous administrated for 4 times every other day. The tumor volume and body weight of mice were both measured, and tumor volume was calculated using Eq. (2):

$$\text{Volume} = \text{Width}^2 \times \text{Length}/2 \quad (2)$$

On Day 16, mice were sacrificed and tumor tissues were collected, weighted. For histological analysis, tumors were harvested, fixed, embedded in paraffin, sliced for H&E staining and TUNEL immunofluorescence with commercially available kits. For CRT and HMGB1 expression, slides of tumor tissues were dewaxed, antigen-repaired, permeabilized, and incubated with primary antibody, secondary antibody, counter stained with Hoechst 33258 and visualized using CLSM.

2.13. ·OH generation in vivo

In vivo ·OH generation was measured using the similar method as *in vitro* ·OH generation assay. Briefly, tumor tissues were homogenized in ice bath and centrifuged at 5000 rpm (Beckman Coulter, Allegra X-30, Kraemer Boulevard Brea, CA, USA) to collect supernatant. Then BA solution (0.5 mmol/L) was added into each sample and incubated for 30 min at room temperature. Finally, the samples were filtered and the absorbance of supernatant was measured at 435 nm.

2.14. Immune cells and cytokines analysis

Tumor tissues from 2.12 were collected and cut into small pieces for immune cell analysis. Tumor tissues were digested with tissue lysis buffer (2 mg/mL of collagenase IV and 1 mg/mL of DNase I) for 1 h at 37 °C. Subsequently, samples were filtered using cell strainer (200 mesh) and washed with PBS three times. The obtained cells were re-suspended in FCSB and cocktail antibodies were added into each sample and detected using flow cytometry (CD3, CD4 and CD8 for $CD4^+$ and $CD8^+$ T cells; CD11b, F4/80 and CD206 for M1 and M2 TAM; CD11c, CD80 and CD86 for matured DCs in tumor-draining lymph nodes). Tumor TNF-α, IFN-γ and IL-6 level were measured using different ELISA kits. Detailed procedure was according to the manufacturer of the kits.

2.15. Safety evaluation

In order to investigate *in vivo* toxicity of different nanoparticles, healthy BALB/c mice were randomly divided into several groups including control, DO-Fe, ADO-Fe, PADO-Fe and PADO-Fe plus aPD-L1, and the concentrations of DOX and aPD-L1 were 2 and 1 mg/kg, respectively. The administration route of nanoparticles and antibody was in the same strategy as *in vivo* antitumor activity assay. During this period, body weight was measured every other day. On Day 16, the mice were sacrificed, and major organs were collected for H&E staining.

2.16. Statistical analysis

Statistical analysis between two groups was performed using one way ANOVA and $P < 0.05$ indicated significant difference.

3. Results and discussion

3.1. Preparation and characterization of PADO-Fe

The ICD amplifier PADO-Fe was prepared through two simple steps including ADO-Fe formation and PEG modification. For preparation of ADO-Fe, DOX, ATP and Fe^{2+} were co-assembled *via* $\pi-\pi$ stacking and coordination force. The lone pair electrons of DOX and ATP make it possible to interact with metal ions and form uniform nanoparticles[40]. Furthermore, drug loading and loading ratio of drugs could be tailored easily through adjusting feeding ratios of drugs and ions. Many DOX-metal ions-based coordination polymer nanoparticles were prepared[41,42], while mono-ATP-based coordination polymer nanoparticles has been rarely reported. Inspired by traditional calcium phosphate nanoparticles (CPNs), which phosphate groups were coordinated with calcium ions for precipitation, we hypothesized whether ATP could serve as a substrate of coordination polymer nanoparticles. As shown in Fig. 1A, different ADO-Fe nanoparticles were prepared with different feeding ratios, with an increase of metal ions from 1:0.5:1 to 1:0.5:5, particle size gradually increased, indicating stronger drug-metal ions interaction was formed and this result fitted the classical nucleation and growth profile of nanocrystalline[42]. When the ratio reached 1:0.5:5, no significant particle size change could be observed, therefore we selected 1:0.5:5 as an optimized feeding ratio and prepared the nanoparticles in the following study. A strange phenomenon was found that during this process mono-ATP/Fe^{2+} could not be easily self-assembled to form cluster aggregation. Although there are many binding sites for metal ions in ATP (including phosphate groups, nitrogen and oxygen atoms of nucleobases), the difficulty of ATP/Fe^{2+} formation is perhaps due to phosphate groups (triphosphate group) bring more negative charges, which form strong electrostatic barrier to interact with metal ions. In the present study, a DOX/ATP co-assembly system ADO-Fe was designed and prepared, besides coordination effect, $\pi-\pi$ stacking force also plays a vital role in the formation of this system, which could significantly increase loading capability of ATP. Due to the presence of

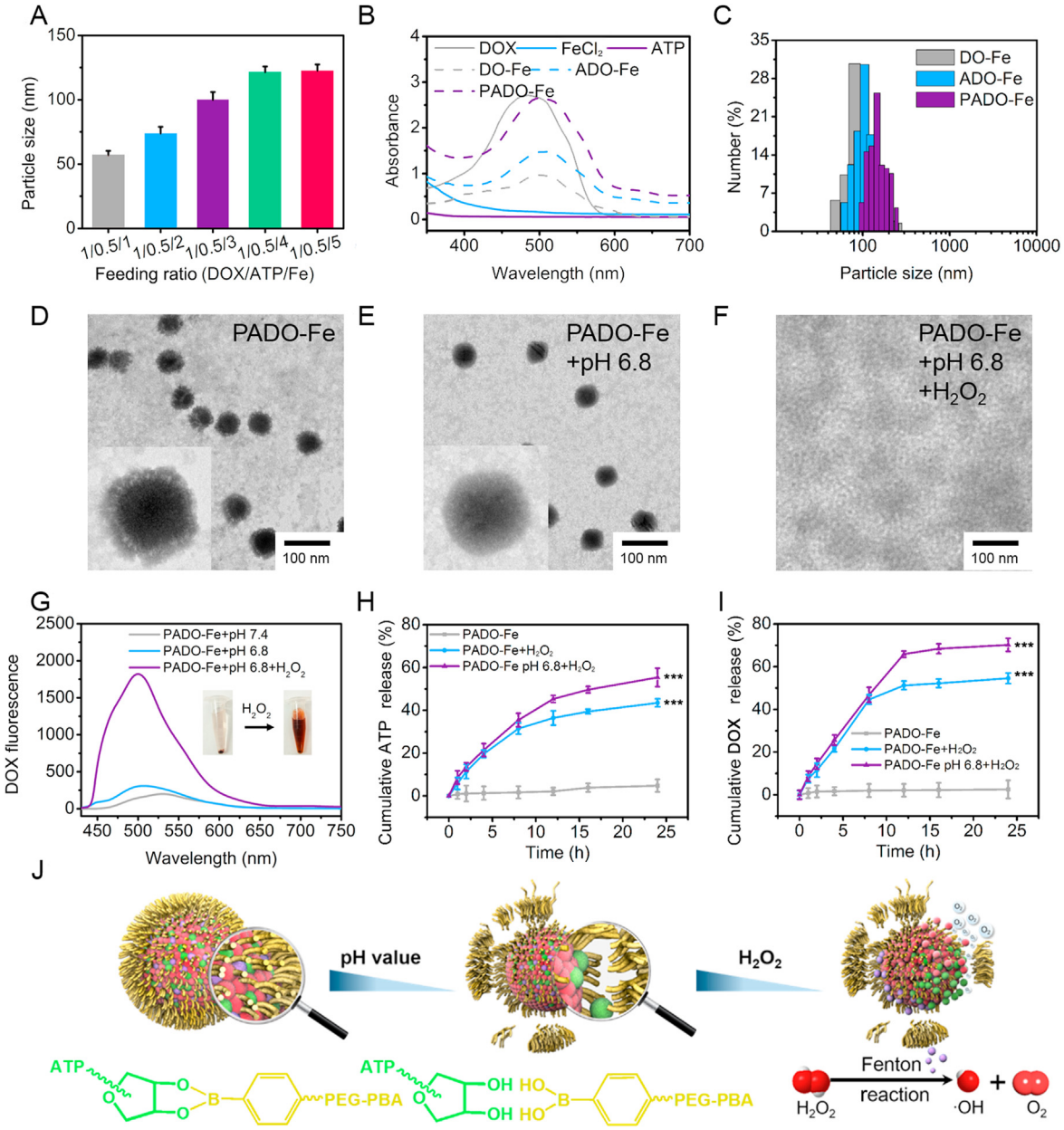

Figure 1 Synthesis and characterization of PADO-Fe. (A) Particle size of various nanoparticles with different feeding ratio; (B) UV−Vis spectra of free DOX, ATP, $FeCl_2$, DO-Fe, ADO-Fe and PADO-Fe in distilled water; (C) particle size distribution of DO-Fe, ADO-Fe and PADO-Fe with feeding ratio of 1:0.5:5; TEM images of PADO-Fe in neutral environment (D), acidic pH (E) and acidic pH plus H_2O_2 (F), scale bars represented 100 nm; (G) fluorescence spectrum of PADO-Fe in different conditions; (H and I) accumulative ATP and DOX release behavior from PADO-Fe in H_2O_2 and H_2O_2 plus pH 6.8; (J) possible mechanism for pH/H_2O_2 dual-responsive drug release behavior of PADO-Fe. Data were presented as mean ± SD and $^{***}P < 0.001$ were considered as statistical difference.

nucleotide residues in ATP, it could also form $\pi-\pi$ stacking force with DOX and was conducive to cluster aggregation and nanoparticles formation.

PADO-Fe was prepared using simple mixing method. Thanks to the vicinal diols structure in D-ribose unit of ATP, which could reversibly bind with phenylboric acid (PBA)[43]. Therefore, PBA-PEG-PBA was synthesized and modified on the surface of ADO-Fe. This PEG shell could not only increase stability and *in vivo* circulation time, but also possess pH-responsive dissociation property and tumor-targeting capability. As displayed in Supporting Information Table S1, the encapsulation efficiency (EE) and full name (LC) of different nanoparticles were measured and EE of three nanoparticles was all over 90% with high LC. In addition, UV−Vis absorbance spectrum was also measured to understand the structure and the formulation of nanoparticles. As shown in Fig. 1B, compared with free DOX, significant red-shift could be observed for three nanoparticles, indicating successful nanoparticle fabrication.

Particle size distribution of three different nanoparticles was measured. As reflected in Fig. 1C, particle size of DO-Fe and ADO-Fe was ~110 nm and a slight increase of particle size could be observed for PADO-Fe (~120 nm) with narrow size

distribution, suggesting all nanoparticles were uniform. Stability assay of different nanoparticles was also performed in PBS at 4 °C (Supporting Information Fig. S1). No obvious particle size change for three nanoparticles during 24 h indicates they are stable for at least 1 day. TEM images of DO-Fe, ADO-Fe and PADO-Fe are displayed in Fig. 1D and Supporting Information Fig. S2, three nanoparticles were solid spheroid or spheroid-like shape with uniform size distribution. The particle sizes of three nanoparticles were consistent with DLS data. To further investigating the verification of PADO-Fe in different conditions, PADO-Fe was placed in pH 6.8 PBS and pH 6.8 PBS + H_2O_2, respectively, and observed using TEM. From Fig. 1E and F, PEG coating of PADO-Fe was removed in acidic pH compared with the physiological environment, indicating PBA-PEG-PBA possessed pH-responsive dissociation capability. Furthermore, no integrated nanoparticle could be observed in both pH and H_2O_2 environment.

In order to investigate the potential mechanism of the disappearance of PADO-Fe, DOX fluorescence was measured in different conditions. As shown in Fig. 1G, characteristic peak of DOX could be observed in both pH and H_2O_2 environment, demonstrating DOX was released from PADO-Fe in these conditions. Moreover, drug release of PADO-Fe was monitored in different stimulations. As illustrated in Fig. 1H and I, under neutral system, negligible DOX/ATP release could be observed during 24 h, which demonstrated its superior stability in physiological condition. By contrast, elevated release profile could be observed for both ATP (42.5%) and DOX (54.8%) in H_2O_2 environment. It is interesting that in H_2O_2+pH 6.8, release profiles of both drugs (70.6% for DOX and 57.7% for ATP) were slightly higher than in neutral pH. This pH-responsive release behavior was attributed to acidic-triggered leakage of borate ester bond from PBA-PEG-PBA and ADO-Fe, which facilitate drug release efficacy.

From the aforementioned results, we proposed possible drug release mechanism of PADO-Fe in different conditions. As given in Fig. 1J, in acidic pH, borate ester bond would break and induce PEG coating de-shielded from ADO-Fe. With the assistance of H_2O_2, Fe^{2+} of ADO-Fe would catalyze H_2O_2 to highly toxic ·OH and O_2 through Fenton reaction. The appearance of microbubbles during Fenton reaction in the interior of nanoparticle would trigger dissociation of PADO-Fe between chemodrugs and Fe^{2+}. These results indicated that PADO-Fe could remain its structure in blood circulation with minor drug leakage, while rapidly release drugs once targeting tumor cells and internalized into cytoplasm of tumor cells. To further investigate our hypothesis, O_2 and ·OH generation assay was investigated, as reflected in Fig. 2A and B, with an increase of incubation time, enhanced generation of O_2 and ·OH could be observed for all nanoparticles, further proving the existence of Fenton reaction. Meanwhile, O_2 generation was also observed using CLSM. As shown in Supporting Information Fig. S5, the decrease of red fluorescence indicated oxygen generation, PADO-Fe possessed the strongest oxygen generation capability with rarely red fluorescence, indicating sufficient PADO-Fe internalization into tumor cells and sufficient Fenton reaction. Of special concern, efficient ·OH generation could possess chemodynamic therapy (CDT) and amplify ICD cascade-based cancer immunotherapy[44].

3.2. *In vitro cellular level assay of PADO-Fe*

To access the cellular uptake capability of PADO-Fe, CLSM and flow cytometry assay were both investigated. For CLSM assay, 4T1 tumor cells were incubated with PADO-Fe, visualized nuclei with Hoechst 33258 and observed using CLSM. Free DOX, DO-Fe and ADO-Fe were served as control. As displayed in Fig. 2C and D, rarely red fluorescence could be observed for DOX group, implying insufficient DOX accumulation into cytoplasm of tumor cells. In contrast, elevated DOX accumulation could be observed for DO-Fe and ADO-Fe, which verifying the enhanced tumor internalization capability of nanoparticles. PADO-Fe possessed the strongest red fluorescence among all reference groups, which was mainly attributed to high affinity between PBA and sialic acid residues. Flow cytometry analysis was also investigated to evaluate cellular uptake level quantitatively. As reflected by Fig. 2E, similar DOX internalization trends were obtained, indicating superior cellular internalization capability of ICD amplifier (PADO-Fe).

After verifying the excellent performance of ICD amplifier, we are aiming to investigate its therapeutical effect *in vitro*. As shown in Fig. 4 and Supporting Information Fig. S3, cell cytotoxicity of blank ATP and $FeCl_2$ was first accessed and no significant cell cytotoxicity could be observed. As displayed in Fig. 2F–H, cell cytotoxicity of ICD amplifier was investigated without/with H_2O_2. IC_{50} of free DOX was approximately 25 μg/mL in both conditions, implying H_2O_2 had no effect in cell proliferation. It is noted that for all Fe-based nanoparticles, IC_{50} with H_2O_2 was lower than without H_2O_2, indicating Fe^{2+}- driven ·OH generation in H_2O_2 environment could also possess cell-killing capability against tumor cells. IC_{50} of both DO-Fe and ADO-Fe was significantly lower than that of free DOX, which was consistent with cellular uptake assay. As expected, PADO-Fe exhibited the highest cell cytotoxicity, demonstrating PADO-Fe could efficiently accumulate into cytoplasm of tumor cells and possess chemotherapy-CDT synergistic therapy, which could achieve enhanced therapeutical outcomes. It is noteworthy that no significant difference could be observed in cell cytotoxicity between DO-Fe and ADO-Fe, demonstrating that ATP could not induce direct cell-killing capability for tumor cells.

Subsequently, anti-proliferation property of ICD amplifier was investigated using annexin V-FITC/PI method. As shown in Fig. 2I and J, ∼15.0% apoptosis positive cells could be observed for both DOX groups, implying moderate apoptosis-inducing effect of free DOX. Notably, elevated apoptosis cells could be observed for DO-Fe and ADO-Fe and this percentage was higher in the presence of H_2O_2. This result might be attributed to higher cellular internalization of nanoparticles and improved therapeutic efficacy of DOX. Furthermore, the generation of highly toxic ·OH would also induce cell apoptosis and possess tumor CDT. As expected, PADO-Fe still exhibited the best apoptosis-inducing effect compared with all other groups, which attributed to the synergistic effect of PBA-mediated active targetability, DOX-induced cell apoptosis and ·OH-induced tumor CDT. These results highlighted the potential therapeutic outcomes of this ICD amplifier for combinational tumor chemotherapy and immunotherapy.

3.3. *ATP-amplified ICD cascade of PADO-Fe*

To explore the potential mechanism of PADO-Fe for ICD amplification, a series of studies were carried out. DCs maturation was first investigated to evaluate immunogenicity of tumor cells after treatment of different nanoparticles. As displayed in Fig. 3A, immature DCs were seeded into the lower chamber while drug-treated 4T1 cells were seeded into the upper chamber. The cells were co-cultured for 12 h and cells of lower chamber were collected and

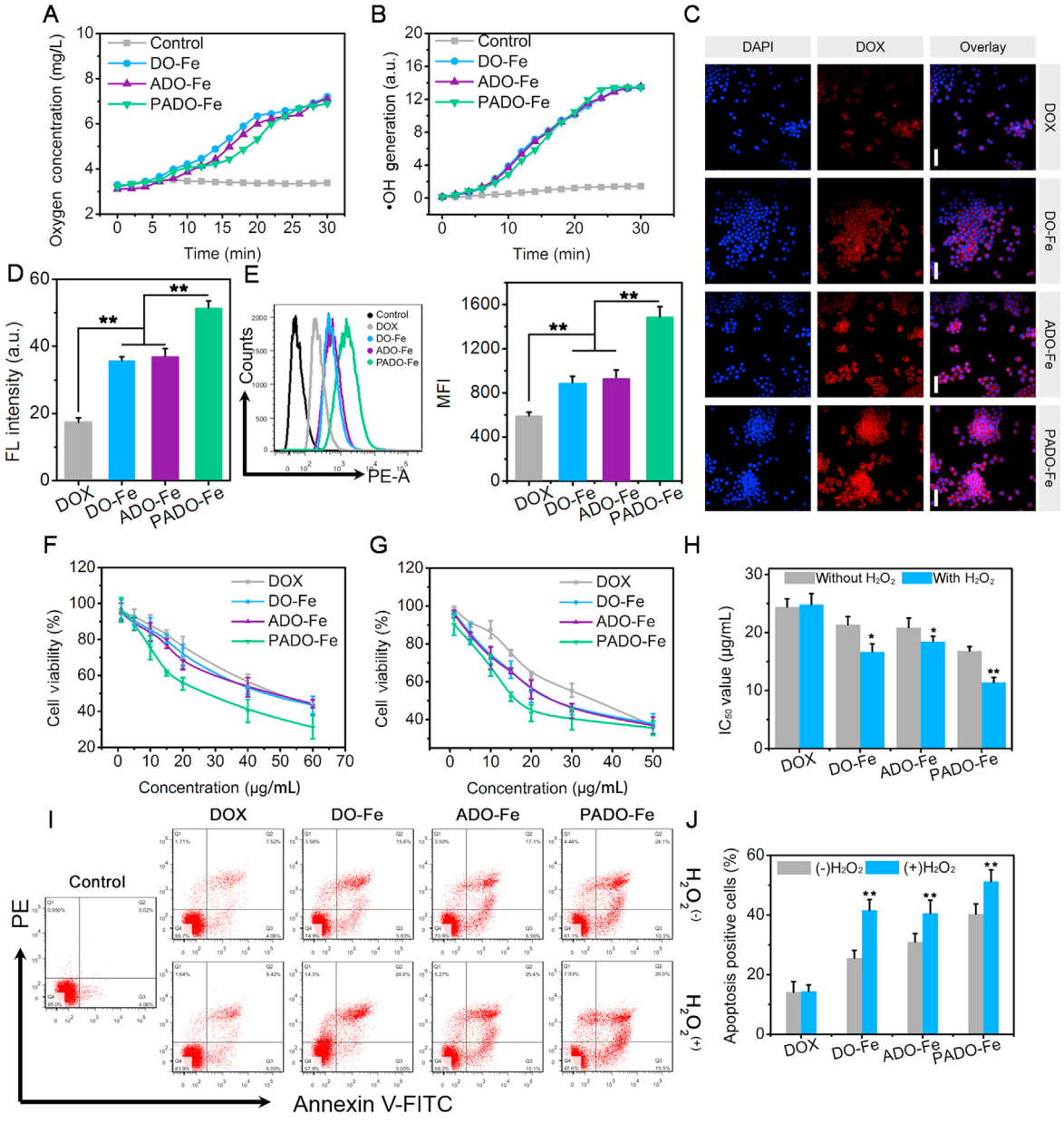

Figure 2 Oxygen (A) and hydroxyl radical (B) generation of different Fe-based nanoparticles in H_2O_2; (C) cellular uptake behavior of different nanoparticles observed by CLSM, red and blue fluorescence represented DOX and nuclei, respectively. Scale bars represented 100 μm; (D) semi-quantitative analysis of the cellular uptake of different nanoparticles; (E) flow cytometry images and histogram analysis of cellular uptake behaviors, concentration of DOX was 10 μg/mL; *in vitro* cell cytotoxicity study of different nanoparticles in the absence (F) and presence (G) of H_2O_2 against 4T1 tumor cell line; (H) IC_{50} value of different nanoparticles with or without H_2O_2; flow cytometry (I) and histogram analysis of the apoptosis cells (J) of 4T1 tumor cells after treatment with DOX, DO-Fe, ADO-Fe and PADO-Fe with or without H_2O_2. Data were presented as mean ± SD and $*P < 0.05$; $**P < 0.01$; were considered as statistical difference.

analyzed by flow cytometry. As described in Fig. 3B, matured DCs percentage was analyzed with flow cytometry (gated as $CD11c^+$ $CD80^+CD86^+$ for matured DCs). Negligible positive cells (~10.5%) were found for blank group, while higher matured DCs percentage for DOX group (~17.0%) implied DOX could increase immunogenicity of tumor cells and induce DCs maturation. Furthermore, no significant influence for DOX group with (~17.8%) or without H_2O_2 implied negligible influence on DCs maturation for H_2O_2 itself. However, for all Fe-based nanoparticles, higher DCs maturation percentage was found in H_2O_2 compared with the absence of H_2O_2, suggesting Fe^{2+} could produce hydroxyl radical in the presence of H_2O_2 through Fenton reaction and induce cancer CDT, which could also induce ICD cascade. Particularly, DO-Fe possessed stronger DCs maturation capability (~20.3%) compared with DOX group, demonstrating higher cellular internalization of DO-Fe. Interestingly, higher matured DCs percentage of ADO-Fe (~31.3%) was found and this result was mainly attributed to the elevated ATP release during the apoptosis process of tumor cells, which played a vital role for DCs recruitment and maturation. As expected, PADO-Fe owned the strongest capability

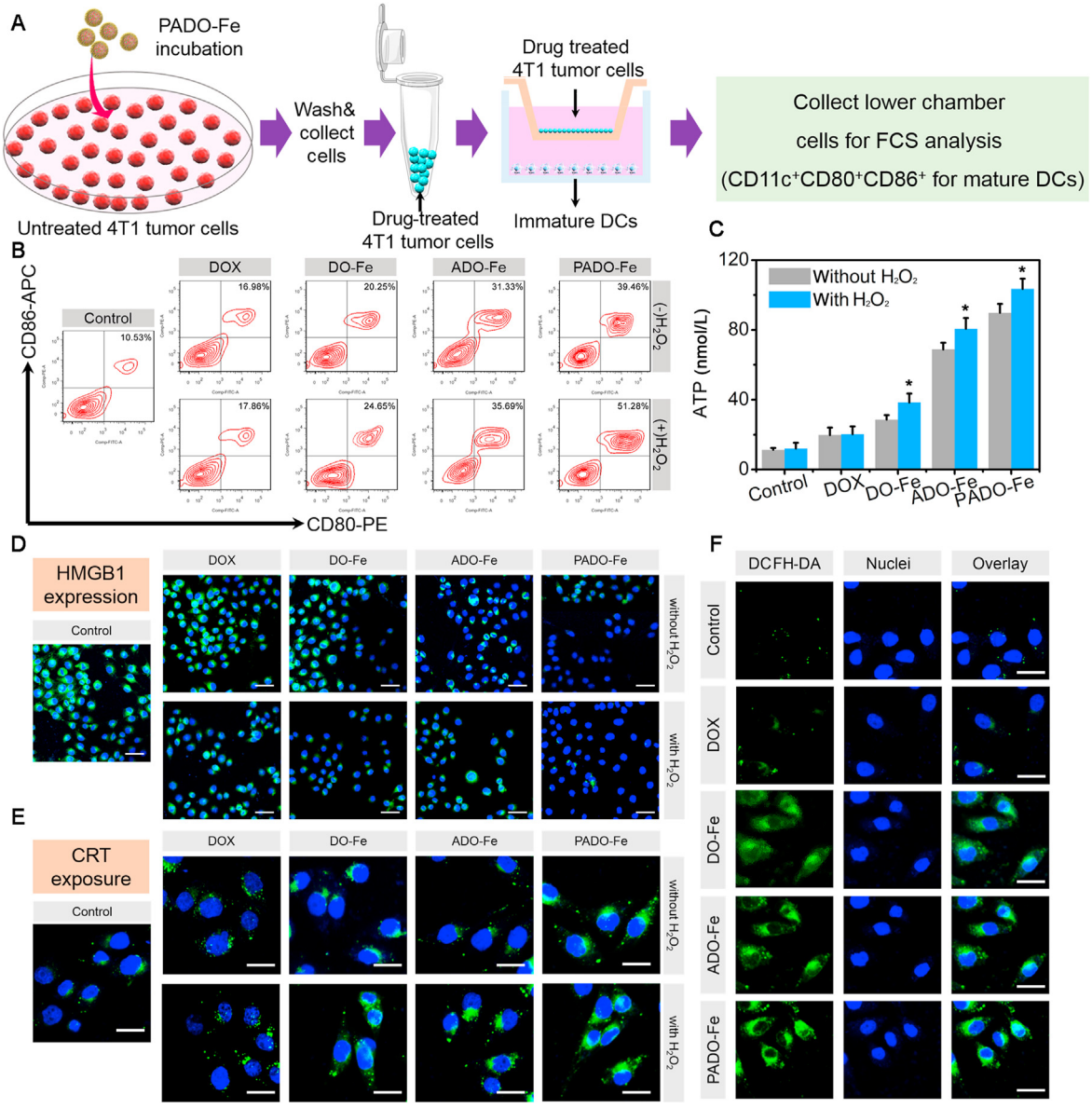

Figure 3 (A) Schematic illustration of Transwell model for DCs maturation analysis; (B) flow cytometry analysis of DCs maturation percentage when tumor cells were treated with DOX, DO-Fe, ADO-Fe and PADO-Fe with or without H_2O_2; (C) extracellular ATP content when tumor cells were treated with different nanoparticles with or without H_2O_2; (D) HMGB1 immunofluorescence after administrated with DOX, DO-Fe, ADO-Fe and PADO-Fe in the presence/absence of H_2O_2, green and blue fluorescence indicated HMGB1 and nuclei, respectively, and scale bars represented 50 μm; (E) CRT immunofluorescence of different groups, green and blue fluorescence indicated CRT and nuclei, scale bars represented 20 μm; (F) hydroxyl radical generation of tumor cells after treatment of different nanoparticles, scale bars represented 20 μm. Data were presented as mean ± SD and $*P < 0.05$ were considered as statistical difference.

for DCs maturation (~51.3% with H_2O_2) due to the synergistic effect of PBA-medicated cellular internalization, Fe-based tumor CDT and rapid DOX release.

To further demonstrate whether this ICD amplifier would enhance ICD cascade, ATP content, CRT and HMGB1 expression were all investigated. As an important 'find me signal', ATP content was measured first. As illustrated in Fig. 3C, negligible ATP concentration was found for control group while it is higher for DOX groups. DO-Fe possessed higher ATP concentration, indicating efficient ICD-inducing effect. Interestingly, ADO-Fe displayed significantly higher ATP content, implying successful ATP delivery and release into cytoplasm of tumor cells, which could facilitate extracellular ATP secretion of dying tumor cells to amplify ICD cascade. Highest ATP concentration was found for PADO-Fe, implying the synergistic effect of ICD-inducing effect.

CRT and HMGB1 expression were also observed by CLSM. As illustrated in Fig. 3D, after treatment of PADO-Fe, significantly higher CRT expression could be observed, indicating successful transportation of CRT to surface after endoplasmic reticulum (ER) stress. In addition, decreased HMGB1 expression was found (Fig. 3E), suggesting effective HMGB1 release. Meanwhile, this effect could be amplified in H_2O_2 environment, indicating the therapeutic outcomes of CDT during ICD cascade. In order to investigate the intracellular hydroxyl radical level, DCFH-DA was

used as a fluorescence probe, which could react with hydroxyl radical and produce green fluorescence. As shown in Fig. 3F, similar to control groups, rarely green fluorescence was found in cytoplasm treated with DOX, implying a negligible impact on hydroxyl radical production. Despite DOX could induce ER stress and increase H_2O_2 production, it could not catalyze H_2O_2 into hydroxyl radical. Notably, cells treated with Fe-based nanoparticles exhibited stronger fluorescence, implying successful decomposition of H_2O_2 into hydroxyl radical *via* Fenton reaction of Fe^{2+}. More importantly, PADO-Fe maximized the intracellular hydroxyl radical level owing to the combined effect of high cell internalization and efficient catalysis capability. Aforementioned results indicated the preponderance of ICD amplifier PADO-Fe for amplifying ICD response and following immune activation and achieving better therapeutic outcomes for cancer chemo-immunotherapy.

3.4. *In vivo antitumor activity*

In order to investigate the *in vivo* antitumor effect of ICD amplifier, tumor-bearing BALB/c mice model was established. *In vivo* biodistribution assay was first carried out and Cy3 DiNHS ester (1%) was added into PADO-Fe through coordination effect and $\pi-\pi$ stacking. After intravenous administration of different Cy3-labeled nanoparticles for 24 h, rarely fluorescence intensity was found for Cy3 group, while relatively higher accumulation in tumor and liver could be observed for DO-Fe and ADO-Fe, indicating these coordination polymer nanoparticles could target tumor tissues *via* EPR effect and ATP had no effect on circulation time. Strongest fluorescence in tumor was found for PADO-Fe, suggesting superior tumor targetability and circulation time of this ICD amplifier. This result was attributed to PBA-PEG-PBA modification on ADO-Fe enhance its *in vivo* stability and tumor cell targetability (Fig. 4A).

The efficient tumor targeting capability of ICD amplifier encouraged us to further investigate its antitumor efficacy *in vivo*. As illustrated in Fig. 4B, tumor-bearing mice were randomly divided into several groups and intravenous administration of different nanoparticles was performed every other day for 4 times. Meanwhile, tumor volume change of mice was monitored and recorded to draw tumor volume change curves. The mean tumor volume changes were calculated and displayed in Fig. 4C, moderate antitumor activity was found in DOX group, indicating free DOX was difficult to accumulate into tumor cells for tumor killing. However, compared with DOX group, DO-Fe displayed much better antitumor effect, indicating DO-Fe could efficiently accumulate into tumor tissues, the combination effect of DOX and Fe^{2+}-based tumor CDT could reach higher tumor-killing capability and activate immune response for cancer immunotherapy. Interestingly, significant higher tumor volume decrease of ADO-Fe could be observed compared with DO-Fe, which strongly highlighted the therapeutic outcomes of ATP during the ICD cascade. Much more ATP release of dying tumor cells when administrated with AOD-Fe, which acted as 'find me signal' and amplified DCs recruitment and maturation, eventually enhance ICD cascade for better therapeutic outcomes. Particularly, PADO-Fe could more efficiently inhibit tumor growth, owing to its advantage for tumor tissue accumulation and tumor cell targetability. Strikingly, strongest tumor growth inhibition was found for PADO-Fe + aPD-L1, which strongly demonstrated the advantage of ICD amplifier in combination with immune checkpoint inhibitor. In addition, tumors from mice were harvested, weighted (Fig. 4D), and PADO-Fe + aPD-L1 could strongly restrain tumor proliferation with minimal tumor volume and weight. Body weight was also measured and calculated (Fig. 4E) and no obvious fluctuations could be observed except DOX group. TUNEL and ki-67 immunofluorescence were both investigated to evaluate the proliferation level of different nanoparticles. As illustrated in Fig. 4F, PADO-Fe + aPD-L1 displayed the strongest apoptosis-inducing capability and proliferation-inhibition, validating the synergistic antitumor immune response of this approach.

3.5. *Immune activation of PADO-Fe in vivo*

Although PADO-Fe could amplify ICD cascade for cancer immunotherapy, hypoxia TIM would lead to insufficient therapeutic outcome. Elevated expression of H_2O_2 and HIF-1α in hypoxia tumor microenvironment would prevent T cell infiltration, cause recruitment/polarization of M2 macrophage and multidrug resistance[45–47]. Therefore, we are interested to seek whether this ICD amplifier could modulate tumor hypoxia. As shown in Fig. 4F and G, HIF-1α expression was measured using Western blotting. Surprisingly, all Fe-based nanoparticles displayed decreased HIF-1α expression, indicating all these nanoparticles could relieve tumor hypoxia. PADO-Fe and PADO-Fe + aPD-L1 displayed the strongest hypoxia relief capability, which was mainly attributed to precise tumor delivery capability of ICD amplifier. We hypothesized that the potential mechanism was because Fenton reaction of Fe^{2+}, which could decompose H_2O_2 into ·OH and O_2. Therefore, we investigated ·OH generation of different nanoparticles. Similarly, significant increase of ·OH generation was found for both PADO-Fe and PADO-Fe + aPD-L1 groups. All these results demonstrated the ICD amplifier PADO-Fe could efficiently relieve tumor hypoxia, which is crucial for TIM reversal and activating antitumor immune response.

To further demonstrate the potential mechanism for antitumor immune response, a series of studies were carried out. CRT and HMGB1 expression were both investigated by CLSM. As shown in Fig. 5A, elevated CRT and decreased HMGB1 expression were found for PADO-Fe, which are important "eat me signal" for ICD cascade. Meanwhile, significantly higher ATP concentration was measured for ADO-Fe compared with DO-Fe (Fig. 5B), suggesting ADO-Fe could efficiently increase ATP release for DCs recruitment. As expected, PADO-Fe + aPD-L1 displayed the highest ATP concentration due to sufficient tumor-targeting delivery and strong antitumor immune response. DCs maturation capability was also measured by flow cytometry. As shown in Fig. 5C and F, significant increase of matured DCs ($CD80^+CD86^+$, gated from $CD11c^+$) was found for ADO-Fe compared with DO-Fe, implying intratumoral delivery of ATP was sufficient for DCs maturation due to higher 'find me signal' release of dying tumor cells.

M2 macrophages is a key biomarker for TIM, which induces tumor hypoxia, insufficient T cell infiltration, multidrug resistance and eventually causes tumor immune tolerance[27,29,31]. As displayed in Fig. 5D and G, strong reduction of M2 macrophage percentage ($CD11b^+F4/80^+CD206^+$) for Fe-based nanoparticles (DO-Fe, ADO-Fe and PADO-Fe) implied Fe could induce TAM polarization from M2 to M1, which was consistent with references reported[48,49]. PADO-Fe + aPD-L1 displayed the highest M1 macrophage subpopulation, suggesting synergistic effect of phenotype polarization and hypoxia relief from Fe and immune checkpoint blockade of aPD-L1. M2 macrophages immunofluorescence was also carried out and illustrated in Fig. 5I. Green, blue and red fluorescence indicated M2 macrophages, vessels and

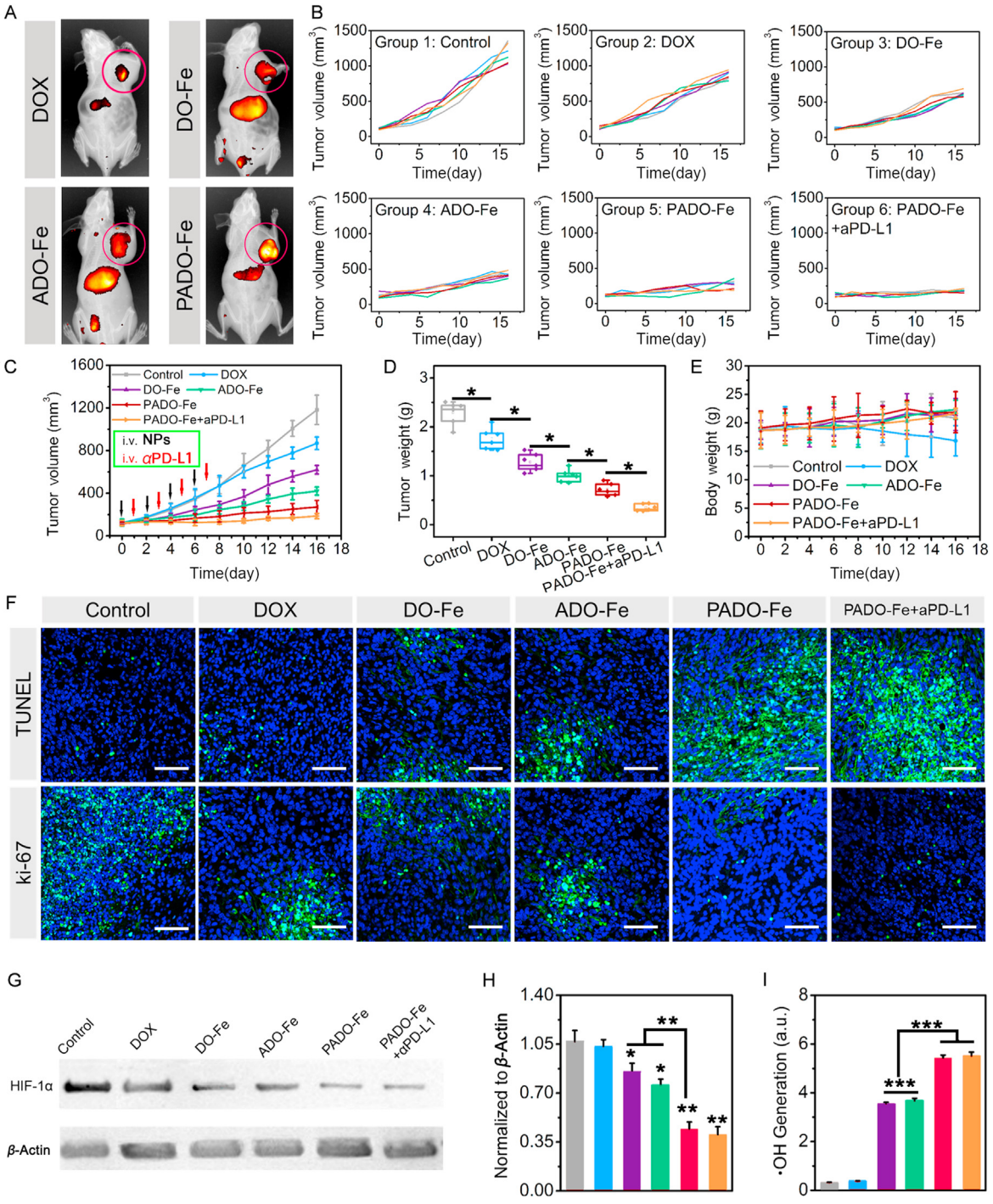

Figure 4 (A) *In vivo* biodistribution study of different Cy3-labeled nanoparticles after intravenous administration for 24 h; individual tumor volume curves (B), mean tumor volume changes (C), tumor weight (D) and body weight changes (E) of mice after treatment with DOX, DO-Fe, ADO-Fe, PADO-Fe and PADO-Fe plus aPD-L1 (2 and 1 mg/kg for DOX and aPD-L1, respectively); (F) TUNEL and ki-67 immunofluorescence of tumor tissues from different drug-treated groups, scale bars represented 100 μm; (G) Western blotting and (H) semi-quantitative analysis of HIF-1α expression from tumor tissues after treatment of various nanoparticles; (I) *in vivo* hydroxyl radical generation after treatment of different nanoparticles. Data were presented as mean ± SD and $^{*}P < 0.05$; $^{**}P < 0.01$; $^{***}P < 0.001$ were considered as statistical difference.

nuclei, respectively. As expected, significant decrease of green pixel dots was found after treatment with PADO-Fe + aPD-L1, which was consistent with flow cytometry data, implying this strategy could efficiently reverse TIM and activate antitumor immune response. Of special concern, we found most M2 macrophages preferentially located in well-perfused regions of tumor.

$CD4^{+}$ and $CD8^{+}$ (CTL, gated from CD3) T cells infiltration was both measured. As reflected on Fig. 5E and H, significantly

elevated CTL and $CD4^+$ T cells could be observed for PADO-Fe compared with control group. Meanwhile, after i. v. injection of aPD-L1, this effect could be amplified. Key cytokines (TNF-α, IFN-γ, IL-6) were measured using ELISA kits and the results were illustrated in Supporting Information Figs. S6−S8. Compared with other groups, significant increase of three cytokines was found in mice treated with PADO-Fe + aPD-L1, verifying this ICD amplifier in combination with immune checkpoint blockade could induce robust pro-inflammatory response. All these results validated successful antitumor immune response of this ICD amplifier.

Based on aforementioned results, we proposed the possible mechanism for synergistic ICD amplifier and immune checkpoint blockade as follows (Fig. 6). PADO-Fe was accumulated into tumor tissues *via* EPR effect and target tumor cells through PBA/sialic acid residues interaction. When PADO-Fe was internalized into cytoplasm, PBA-PEG-PBA shell would dissociate from ADO-Fe *via* breakage of borate ester bonds. In combination with high H_2O_2 concentration, Fe^{2+} would catalyze H_2O_2 to highly toxic ·OH and O_2 through Fenton reaction, which could induce tumor CDT and relieve tumor hypoxia. Furthermore, oxygen microbubbles played a vital role for DOX and ATP release for cell killing and increasing immunogenicity of tumor cells. Significantly higher ATP level would bring stronger 'find me signal' for DCs recruitment, accomplished by multi-components tumor-associated antigens (TAAs)-stimulated DCs maturation and

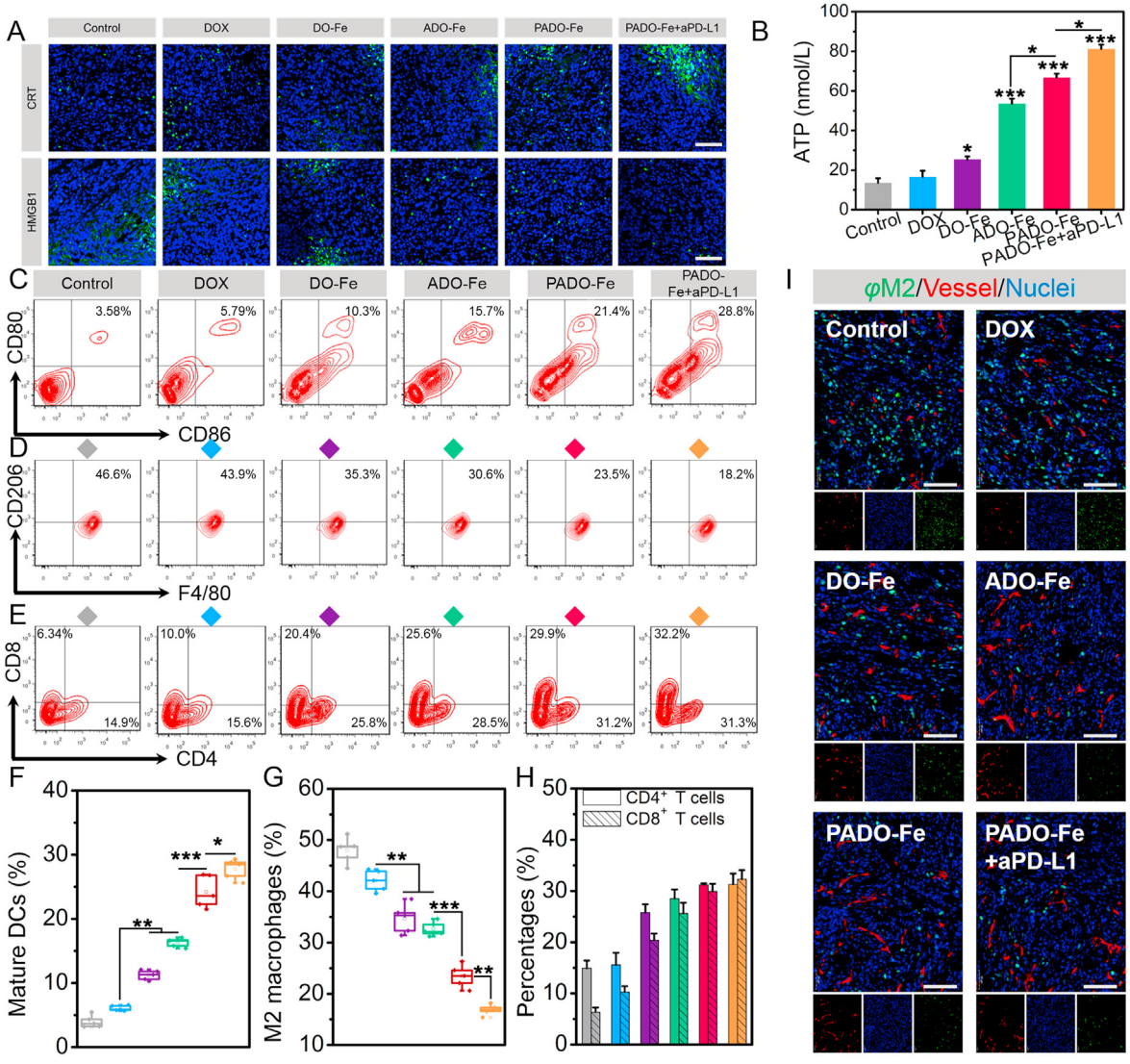

Figure 5 (A) CRT and HMGB1 expression of tumor tissues after treatment of various nanoparticles; scale bars represented 100 μm; (B) ATP content of solid tumors after treatment of different formulations; (C and F) flow cytometry and quantitative analysis of *in vivo* matured DCs percentage of tumor-draining lymph node; (D and G) flow cytometry and quantitative analysis of M2 macrophages percentage of tumor tissues after various treatments; (E and H) flow cytometry and quantitative analysis of $CD4^+$ and $CD8^+$ T cells infiltration of tumor tissues after various treatments; (I) immunofluorescence analysis of M2 macrophage percentage and distribution of tumor tissues after treatment with DOX, DO-Fe, ADO-Fe, PADO-Fe and PADO-Fe plus aPD-L1, green, red and blue fluorescence indicated M2 macrophages, tumor vessels and nuclei, respectively, scale bars represented 100 μm. Data were presented as mean ± SD and $^*P < 0.05$; $^{**}P < 0.01$; $^{***}P < 0.001$ were considered as statistical difference.

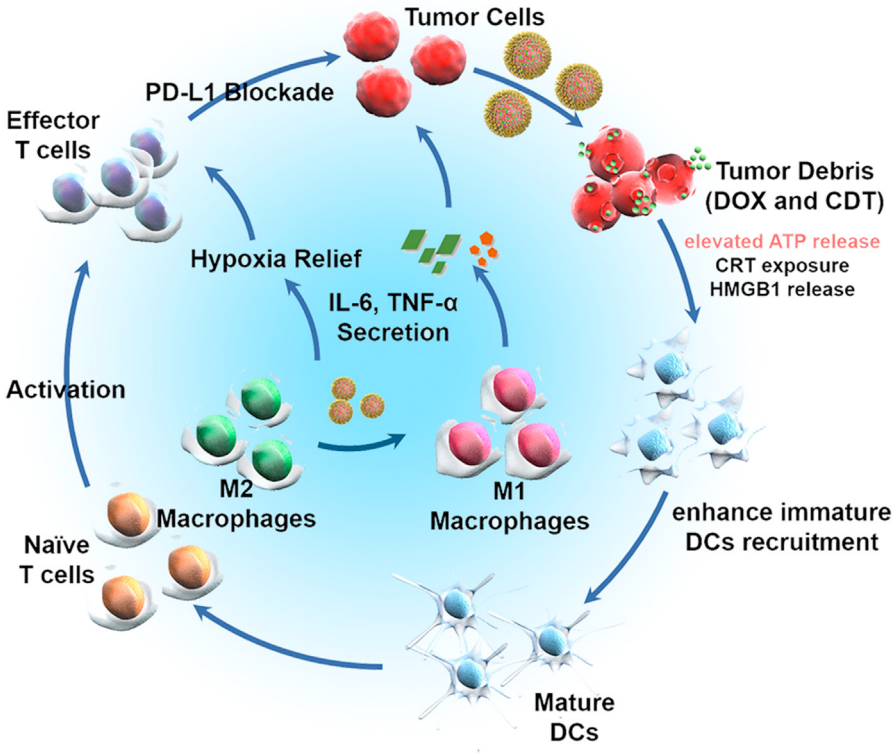

Figure 6 Possible mechanism for ICD induction in combination with PD-L1 immune checkpoint blockade for ICD amplifier PADO-Fe.

antigen presenting. On the other hand, Fe^{2+} would also induce polarization of TAM from M2 to M1 and reverse TIM. The synergistic effect of PADO-Fe can strongly activate T cell infiltration. By the virtue of aPD-L1 for immune checkpoint blockade, PADO-Fe could efficiently activate antitumor immune response for cancer chemotherapy-sensitized immunotherapy.

3.6. Primary and distant tumor inhibition

To further explore whether PADO-Fe could activate immune response, a bilateral model of 4T1 tumors was established as described in Fig. 7A. Different nanoparticles were intertumorally injected into the primary tumor every other day for 4 times and allow recovery. Tumor volume of both primary tumor and distant tumor were calculated. As shown in Fig. 7B−D, significant regression for primary tumor could be observed for PADO-Fe + aPD-L1 group, indicating favorable antitumor activity of this nanoparticle. Of special note, the antitumor activity against primary tumor was slightly higher than intravenous administration and this phenomenon was mainly attributed to insufficient tumor accumulation by intravenous administration. To investigate the immune activation capability of ICD amplifier, volume and weight of distant tumor were also accessed. As reflected in Fig. 7E−G, PADO-Fe displayed satisfied antitumor activity against distant tumor and this effect could be elevated after administration of aPD-L1. This encouraging result demonstrated that PADO-Fe could efficiently activate antitumor immune response for cancer immunotherapy.

We hypothesized the reduction of distant tumor volume was mainly attributed to the activation of antitumor immunity. Therefore, a series of studies were investigated against distant tumor. As shown in Fig. 7H, H&E staining of distant tumor was accessed. Most voids and decrease of nuclei were found for PADO-Fe + aPD-L1 group, implying sufficient tumor cell killing and proliferation inhibition. DCs maturation of distant tumor was also accessed. As displayed in Supporting Information Fig. S9, elevated matured DCs percentage of PADO-Fe + aPD-L1 group validated the successful activation of antitumor immune response. $CD8^+$ T cell was stained by immunofluorescence and observed using CLSM. Increased green fluorescence further confirmed sufficient T cell infiltration and antitumor immune response. As reflected on Fig. 7I and J, T cell infiltration of distant tumor was also evaluated by flow cytometry and similar results could be obtained. Key cytokines of distant tumor were also measured using ELISA kit. As shown in Supporting Information Figs. S10−S12, elevated TNF-α, IFN-γ, IL-6 level in distant tumor tissues further implied the antitumor immune response activation of this ICD amplifier.

3.7. Safety evaluation

Safety evaluation was investigated using healthy mice and multi-intravenous administration with various nanoparticles. As shown in Supporting Information Fig. S13 and S14, no obvious weight loss for all groups indicated the tolerable side effect for all nanoparticles. Meanwhile, no obvious histological verification of

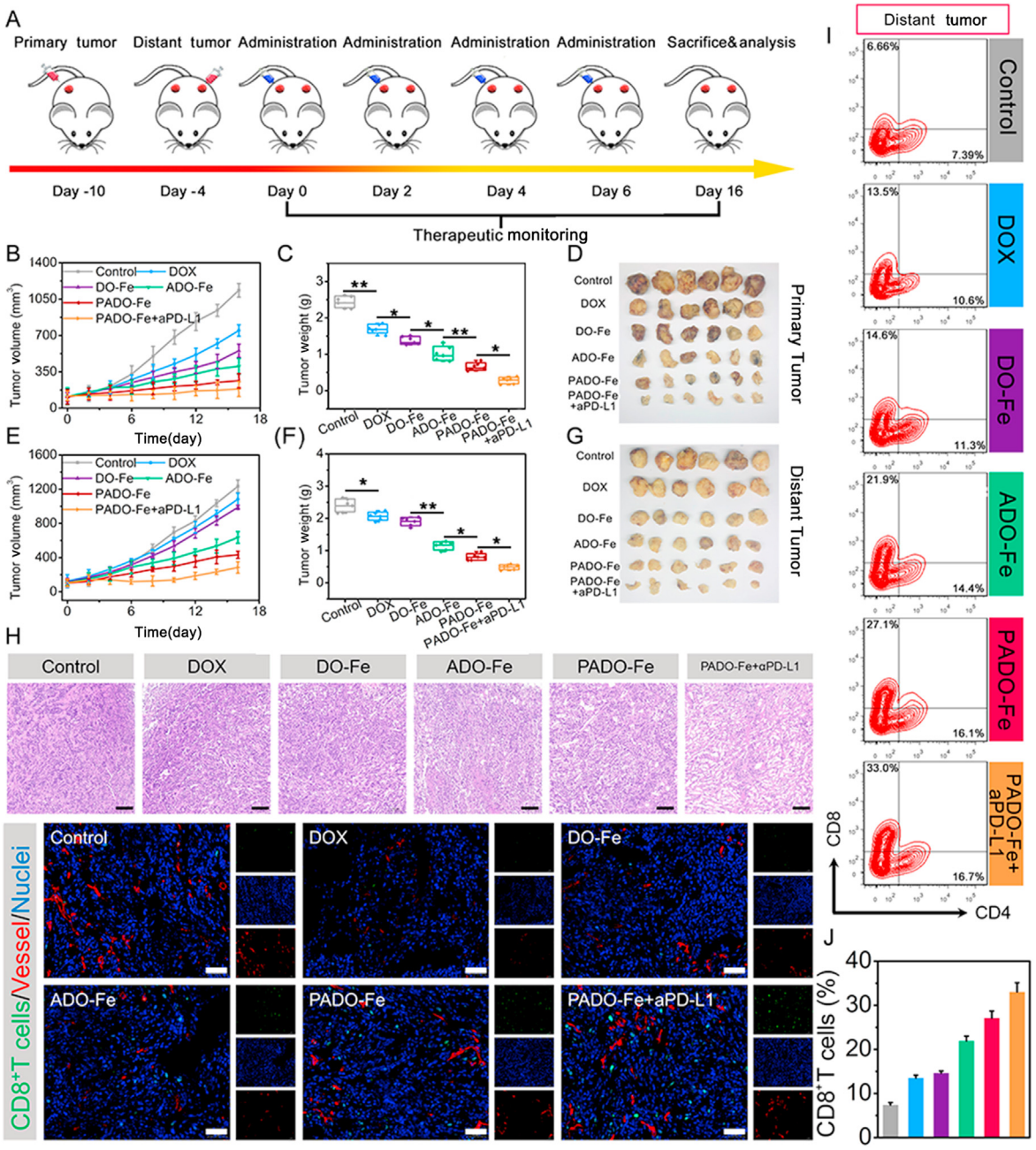

Figure 7 (A) Time schedule of PADO-Fe for primary and distant tumor inhibition; primary tumor volume changes (B), tumor weight changes (C) and tumor photograph (D) of mice after treatment with DOX, DO-Fe, ADO-Fe, PADO-Fe and PADO-Fe plus aPD-L1; distant tumor volume changes (E), tumor weight changes (F) and tumor photograph (G) of mice after treatment with various nanoparticles; (H) H&E and $CD8^+$ T cells infiltration analysis from distant tumors by CLSM, scale bars represented 100 μm; (I and J) flow cytometry and quantitative analysis of $CD4^+$ and $CD8^+$ T cells infiltration of distant tumor tissues after various treatments. Data were presented as mean ± SD and $^*P < 0.05$; $^{**}P < 0.01$ were considered as statistical difference.

major organs further verified this ICD amplifier is safe nanoplatform for cancer management.

4. Conclusions

In summary, a pH/H_2O_2-responsive ICD amplifier, PADO-Fe, was successfully fabricated, which could amplify ICD cascade to enhance immune response to PD-L1 immune checkpoint blockade immunotherapy. By the virtue of $\pi-\pi$ stacking and coordination effect between DOX, ATP and Fe^{2+}, the self-assemblied ADO-Fe owed uniform size distribution and preferable stability. Thanks to the smart molecule structure of ATP, PBA-PEG-PBA could modify on the surface of ADO-Fe *via* borate ester bonds to form PADO-Fe, which could not only increase blood circulation time, but also possess tumor-targeting capability. Besides, PADO-Fe owned favorable tumor targeting, cellular uptake and pH/H_2O_2 dual-responsive drug release behavior, which could efficiently kill

tumor cells and induce ICD response. Of special note, ATP would serve as an ICD "adjuvant", which could amplify "find me signal" to increase DCs recruitment and maturation and amplify ICD cascade. Fe^{2+} of PADO-Fe could not only induce phenotype transition of TAM from M2 to M1, the occurrence of Fenton reaction would also generate O_2 and hydroxyl radical, which could reverse TIM and induce tumor CDT, which eventually induce T cells activation and infiltration in both primary tumor and distant tumor. Collectively, our ICD amplifier may provide a potential approach for enhancing tumor ICD therapy and open a new window for chemotherapy-sensitized immunotherapy.

Acknowledgments

The authors are grateful for the financial support of Natural Science Foundation of China (Nos. 82104108, 82073797, 81874305 and 81773668), China Postdoctoral Science Foundation (2021M693869) and Liaoning Natural Science Foundation for Planned Project (2021JH6/10500161, China).

Author contributions

Jiulong Zhang and Xiaoyan Sun were responsible for all experiments and original draft preparation; Xiufeng Zhao, Menghao Shi, Benzhuo Zhang, and Dawei Chen partly investigated in experiments; Haiyang Hu and Mingxi Qiao were responsible for statistical data analysis; Chunrong Yang, Jiulong Zhang and Xiuli Zhao were responsible for the financial support; Xiuli Zhao was responsible for conceptualization, writing-review, validation and supervision.

Conflicts of interest

The authors declare no conflicts of interest.

Appendix A. Supporting information

Supporting data to this article can be found online at https://doi.org/10.1016/j.apsb.2022.05.008.

References

1. Kang M, Hong J, Jung M, Kwon SP, Song SY, Kim HY, et al. T-Cell-Mimicking nanoparticles for cancer immunotherapy. *Adv Mater* 2020;**32**:2003368.
2. Wang S, Hu X, Wei W, Ma G. Transformable vesicles for cancer immunotherapy. *Adv Drug Deliv Rev* 2021:113905.
3. Chen XS, Moon JJ, Cheon J. New opportunities in cancer immunotherapy and theranostics. *Acc Chem Res* 2020;**53**:2763−4.
4. Mi Y, Smith CC, Yang F, Qi Y, Roche KC, Serody JS, et al. A dual immunotherapy nanoparticle improves T-cell activation and cancer immunotherapy. *Adv Mater* 2018;**30**:1706098.
5. Shi Y, Lammers T. Combining nanomedicine and immunotherapy. *Acc Chem Res* 2019;**52**:1543−54.
6. Chen Y, Wang L, Zheng M, Zhu C, Wang G, Xia Y, et al. Engineered extracellular vesicles for concurrent Anti-PDL1 immunotherapy and chemotherapy. *Bioact Mater* 2022;**9**:251−65.
7. Zhu Y, Yu X, Thamphiwatana SD, Zheng Y, Pang Z. Nanomedicines modulating tumor immunosuppressive cells to enhance cancer immunotherapy. *Acta Pharm Sin B* 2020;**10**:2054−74.
8. de Streel G, Bertrand C, Chalon N, Liénart S, Bricard O, Lecomte S, et al. Selective inhibition of TGF-β1 produced by GARP-expressing Tregs overcomes resistance to PD-1/PD-L1 blockade in cancer. *Nat Commun* 2020;**11**:4545.
9. Luo L, Zhu C, Yin H, Jiang M, Zhang J, Qin B, et al. Laser immunotherapy in combination with perdurable PD-1 blocking for the treatment of metastatic tumors. *ACS Nano* 2018;**12**:7647−62.
10. Chen J, Fang H, Hu Y, Wu J, Zhang S, Feng Y, et al. Combining mannose receptor mediated nanovaccines and gene regulated PD-L1 blockade for boosting cancer immunotherapy. *Bioact Mater* 2022;**7**:167−80.
11. Liu X, Ye N, Liu S, Guan J, Deng Q, Zhang Z, et al. Hyperbaric oxygen boosts PD-1 antibody delivery and T cell infiltration for augmented immune responses against solid tumors. *Adv Sci* 2021;**8**:2100233.
12. Xie L, Wang G, Sang W, Li J, Zhang Z, Li W, et al. Phenolic immunogenic cell death nanoinducer for sensitizing tumor to PD-1 checkpoint blockade immunotherapy. *Biomaterials* 2021;**269**:120638.
13. Chen Q, He Y, Wang Y, Li C, Zhang Y, Guo Q, et al. Penetrable nanoplatform for "cold" tumor immune microenvironment reeducation. *Adv Sci* 2020;**7**:2000411.
14. Fan Z, Liu H, Xue Y, Lin J, Fu Y, Xia Z, et al. Reversing cold tumors to hot: an immunoadjuvant-functionalized metal-organic framework for multimodal imaging-guided synergistic photo-immunotherapy. *Bioact Mater* 2021;**6**:312−25.
15. Xiong X, Zhao J, Su R, Liu C, Guo X, Zhou S. Double enhancement of immunogenic cell death and antigen presentation for cancer immunotherapy. *Nano Today* 2021;**39**:101225.
16. Wang Y, Wang Z, Chen B, Yin Q, Pan M, Xia H, et al. Cooperative self-assembled nanoparticle induces sequential immunogenic cell death and toll-like receptor activation for synergistic chemo-immunotherapy. *Nano Lett* 2021;**21**:4371−80.
17. Martins I, Wang Y, Michaud M, Ma Y, Sukkurwala AQ, Shen S, et al. Molecular mechanisms of ATP secretion during immunogenic cell death. *Cell Death Differ* 2014;**21**:79−91.
18. Duan X, Chan C, Lin W. Nanoparticle-mediated immunogenic cell death enables and potentiates cancer immunotherapy. *Angew Chem Int Ed* 2019;**58**:670−80.
19. Wang Y, Gao D, Liu Y, Guo X, Chen S, Zeng L, et al. Immunogenic-cell-killing and immunosuppression-inhibiting nanomedicine. *Bioact Mater* 2021;**6**:1513−27.
20. Hayashi K, Nikolos F, Lee YC, Jain A, Tsouko E, Gao H, et al. Tipping the immunostimulatory and inhibitory DAMP balance to harness immunogenic cell death. *Nat Commun* 2020;**11**:6299.
21. Banstola A, Poudel K, Kim JO, Jeong J-H, Yook S. Recent progress in stimuli-responsive nanosystems for inducing immunogenic cell death. *J Control Release* 2021;**337**:505−20.
22. Phuengkham H, Ren L, Shin IW, Lim YT. Nanoengineered immune niches for reprogramming the immunosuppressive tumor microenvironment and enhancing cancer immunotherapy. *Adv Mater* 2019;**31**:1803322.
23. Nie W, Yu T, Liu X, Wang B, Li T, Wu Y, et al. Non-viral vector mediated CKb11 with folic acid modification regulates macrophage polarization and DC maturation to elicit immune response against cancer. *Bioact Mater* 2021;**6**:3678−91.
24. Chen X, Pan X, Zhang W, Guo H, Cheng S, He Q, et al. Epigenetic strategies synergize with PD-L1/PD-1 targeted cancer immunotherapies to enhance antitumor responses. *Acta Pharm Sin B* 2020;**10**:723−33.
25. Wei J, Long Y, Guo R, Liu X, Tang X, Rao J, et al. Multifunctional polymeric micelle-based chemo-immunotherapy with immune checkpoint blockade for efficient treatment of orthotopic and metastatic breast cancer. *Acta Pharm Sin B* 2019;**9**:819−31.
26. Kiaie SH, Sanaei MJ, Heshmati M, Asadzadeh Z, Azimi I, Hadidi S, et al. Immune checkpoints in targeted-immunotherapy of pancreatic cancer: new hope for clinical development. *Acta Pharm Sin B* 2021;**11**:1083−97.
27. Chayanon N, Heather HG, Suzie HP. Progress in tumor-associated macrophage (TAM)-targeted therapeutics. *Adv Drug Deliv Rev* 2017;**114**:206−21.
28. Shen S, Li H, Chen K, Wang Y, Yang X, Lian Z, et al. Spatial targeting of tumor-associated macrophages and tumor cells with a pH-sensitive

cluster nanocarrier for cancer chemoimmunotherapy. *Nano Lett* 2017;**17**:3822−9.
29. Singh Y, Kumar P, MeherJaya G, Raval K, Kumar A, Shrivastava R, et al. Targeting tumor associated macrophages (TAMs) via nanocarriers. *J Control Release* 2017;**254**:92−106.
30. Guo N, Zhou Y, Wang T, Lin M, Chen J, Zhang Z, et al. Specifically eliminating tumor-associated macrophages with an extra- and intracellular stepwise-responsive nanocarrier for inhibiting metastasis. *ACS Appl Mater Interfaces* 2020;**12**:57798−809.
31. Cheng Y, Song S, Wu P, Lyu B, Qin M, Sun Y, et al. Tumor associated macrophages and TAMs-based anti-tumor nanomedicines. *Advanced Healthcare Materials* 2021:2100590. n/a.
32. Barenholz Y. Doxil® — the first FDA-approved nano-drug: lessons learned. *J Control Release* 2012;**160**:117−34.
33. Meng X, Zhang F, Guo H, Zhang C, Hu H, Wang W, et al. One-pot approach to Fe2+/Fe3+-based MOFs with enhanced catalytic activity for Fenton reaction. *Advanced Healthcare Materials* 2021:2100780. n/a.
34. Tang Z, Liu Y, He M, Bu W. Chemodynamic therapy: tumour microenvironment-mediated Fenton and fenton-like reactions. *Angew Chem Int Ed* 2019;**58**:946−56.
35. Rojas JM, Sanz-Ortega L, Mulens-Arias V, Gutiérrez L, Pérez-Yagüe S, Barber DF. Superparamagnetic iron oxide nanoparticle uptake alters M2 macrophage phenotype, iron metabolism, migration and invasion. *Nanomed Nanotechnol Biol Med* 2016;**12**:1127−38.
36. Zanganeh S, Hutter G, Spitler R, Lenkov O, Mahmoudi M, Shaw A, et al. Iron oxide nanoparticles inhibit tumour growth by inducing pro-inflammatory macrophage polarization in tumour tissues. *Nat Nanotechnol* 2016;**11**:986−94.
37. Qian Y, Qiao S, Dai Y, Xu G, Dai B, Lu L, et al. Molecular-targeted immunotherapeutic strategy for melanoma via dual-targeting nanoparticles delivering small interfering RNA to tumor-associated macrophages. *ACS Nano* 2017;**11**:9536−49.
38. Sun XY, Zhang JL, Yang CR, Huang ZY, Shi MH, Pan S, et al. Dual-responsive size-shrinking nanocluster with hierarchical disassembly capability for improved tumor penetration and therapeutic efficacy. *ACS Appl Mater Interfaces* 2019;**11**:11865−75.
39. Kong F, Bai H, Ma M, Wang C, Xu H, Gu N, et al. Fe3O4@Pt nanozymes combining with CXCR4 antagonists to synergistically treat acute myeloid leukemia. *Nano Today* 2021;**37**:101106.
40. Zhao J, Bao X, Meng T, Wang S, Lu S, Liu G, et al. Fe(II)-driven self-assembly of enzyme-like coordination polymer nanoparticles for cascade catalysis and wound disinfection applications. *Chem Eng J* 2021:420.
41. Zhao L-P, Zheng R-R, Huang J-Q, Chen X-Y, Deng F-A, Liu Y-B, et al. Self-delivery photo-immune stimulators for photodynamic sensitized tumor immunotherapy. *ACS Nano* 2020;**14**:17100−13.
42. Geng Z, Chen F, Wang X, Wang L, Pang Y, Liu J. Combining anti-PD-1 antibodies with Mn(2+)-drug coordinated multifunctional nanoparticles for enhanced cancer therapy. *Biomaterials* 2021;**275**:120897.
43. Cao J, Gao X, Cheng M, Niu X, Li X, Zhang Y, et al. Reversible shielding between dual ligands for enhanced tumor accumulation of ZnPc-loaded micelles. *Nano Lett* 2019;**19**:1665−74.
44. Ding B, Zheng P, Jiang F, Zhao Y, Wang M, Chang M, et al. MnOx nanospikes as nanoadjuvants and immunogenic cell death drugs with enhanced antitumor immunity and antimetastatic effect. *Angew Chem Int Ed* 2020;**59**:16381−4.
45. Wang B, Zhao Q, Zhang Y, Liu Z, Zheng Z, Liu S, et al. Targeting hypoxia in the tumor microenvironment: a potential strategy to improve cancer immunotherapy. *J Exp Clin Cancer Res* 2021;**40**:24.
46. Zhang Y, Chen H, Wang H, Wang T, Pan H, Ji W, et al. A synergistic cancer immunotherapy nano-system for preventing tumor growth. *Chem Eng J* 2020;**380**:122472.
47. Gao S, Yang X, Xu J, Qiu N, Zhai G. Nanotechnology for boosting cancer immunotherapy and remodeling tumor microenvironment: the horizons in cancer treatment. *ACS Nano* 2021;**15**:12567−603.
48. Chen L, Ma X, Dang M, Dong H, Hu H, Su X, et al. Simultaneous T cell activation and macrophage polarization to promote potent tumor suppression by iron oxide-embedded large-pore mesoporous organosilica core-shell nanospheres. *Adv Healthc Mater* 2019;**8**:e1900039.
49. Wu X, Cheng Y, Zheng R, Xu K, Yan J, Song P, et al. Immunomodulation of tumor microenvironment by arginine-loaded iron oxide nanoparticles for gaseous immunotherapy. *ACS Appl Mater Interfaces* 2021;**13**:19825−35.